

# Stress, microstructure, and stability of Mo/Si, W/Si, and Mo/C multilayer films

David L. Windt<sup>a)</sup>

*Bell Laboratories, Lucent Technologies, Murray Hill, New Jersey 07974*

(Received 28 April 1999; accepted 24 January 2000)

The stresses in periodic Mo/Si, W/Si, and Mo/C multilayer films were determined from wafer-curvature measurements. The layer thickness of each material was varied systematically, and parametric stress contours were generated, showing contours of constant stress in the two-dimensional layer thickness parameter space. These results illustrate that the net stress in a periodic multilayer is not an intrinsic property of the film (for specific deposition conditions) but, rather, depends strongly on the individual layer thicknesses. X-ray diffraction measurements show (a) how the lattice spacing in the W and Mo crystallites varies with layer thickness, and (b) in the case of the W/Si films, how the phase composition of the polycrystalline W layers vary with W layer thickness. In the case of the W/Si and Mo/Si multilayers, irreversible stress changes were observed after the samples were stored in air at room temperature for a period of several months. Stress-temperature measurements made on the as-deposited W/Si and Mo/Si samples also reveal irreversible stress changes (both positive and negative, depending on the layer thicknesses) after thermal cycling to 300 °C; x-ray diffraction measurements were used to identify any associated changes in the W and Mo microstructure. We describe mechanisms that can explain the observed stress behavior, and also discuss the significance of these results, particularly with regard to the use of these films for high-performance multilayer x-ray optics. © 2000 American Vacuum Society. [S0734-2101(00)01703-6]

## I. INTRODUCTION

The rapid advancement over the last decade in the development of multilayer x-ray optics has led to a variety of applications in science and technology in such diverse fields as solar physics and high-energy astrophysics, instrumentation for synchrotron radiation, plasma physics, and photolithography. Understanding and ultimately controlling the stresses in x-ray multilayer coatings is of critical importance for many of these applications since large residual stresses (or large changes in stress over time) can have a deleterious effect on film adhesion and can cause unwanted substrate deformation. Substrate deformation is a particular concern in the case of diffraction-limited x-ray optics (now being developed for photolithography, solar physics, and astronomical x-ray interferometry), where film stress of only a few hundred MPa can distort the x-ray mirror surface by many nanometers (depending on the thickness and composition of the substrate).

A large number of experimental investigations have been reported previously that were directed at understanding the stresses in sputter-deposited single-layer films, with particular emphasis on the variations in stress with deposition conditions, i.e., working gas species and pressure, deposition geometry, substrate bias, substrate temperature, and so forth.<sup>1-10</sup> Previous efforts to understand the stresses in multilayer films have largely focused on the variations in stress with the deposition conditions as well,<sup>11-13</sup> on the mechanisms governing the stress changes as a function of

temperature,<sup>14-16</sup> or on the evolution of stress during growth.<sup>17</sup> In this work, we describe measurements directed chiefly at understanding the variation of multilayer film stress as a function of the thicknesses of the individual layers that comprise the multilayer, how these stresses change with time and temperature, and how they are correlated to the microstructure.

Film stresses were measured using the wafer-curvature technique in as-deposited Mo/Si, W/Si, and Mo/C multilayer structures. The layer thickness of each material was varied systematically, and parametric stress contours were generated, showing contours of constant stress in the two-dimensional layer thickness parameter space. X-ray diffraction (XRD) was used to identify phases present in the polycrystalline metal layers, and to measure the out-of-plane lattice spacing and grain size of these crystallites. In the case of the W/Si and Mo/Si films, the film stress was also measured as a function of temperature during thermal cycling to 300 °C, and postanneal XRD was used to measure any subsequent changes in microstructure.

Following a description of the experimental techniques in Sec. II, we present the results of this investigation in Sec. III. In Sec. IV, we discuss various mechanisms that can explain the results, and conclude in Sec. V with a discussion of the significance of these results, particularly with regard to the production of low-stress, high-performance multilayer x-ray optics.

## II. EXPERIMENT

Multilayer films were grown on polished, 100- $\mu$ m-thick, 76-mm-diam Si(100) wafers by dc magnetron sputtering in argon of 99.999% purity, using a deposition system that has

<sup>a)</sup>Current address: Astrophysics Laboratory, Columbia University, 550 West 120th St., New York, NY 10027; electronic mail: windt@astro.columbia.edu

been described previously.<sup>18</sup> In all cases, the vacuum system reached a background pressure of  $5.0 \pm 0.1 \times 10^{-6}$  Torr prior to deposition, and the argon pressure was fixed at  $1.50 \pm 0.01$  mTorr during deposition. The power applied to each of the two 50-cm-long  $\times$  9-cm-wide planar magnetrons was held constant at 200 W, and the individual film thicknesses were adjusted by varying the (computer-controlled) rotational velocity of the substrate (which faces downward) as it rotated over the sources (which face upward, 10 cm below the plane of the substrate). The deposition rates for Mo (99.95% target purity), W (99.95% purity), Si (99.9% purity), and C (99.999% purity), computed from film thicknesses determined by x-ray reflectance measurements,<sup>19</sup> were found to be approximately 0.25, 0.22, 0.19, and 0.05 nm/s, respectively. The film thicknesses were varied systematically as follows: in the case of Mo/Si, the Mo and Si layer thicknesses both ranged from 1 to 5 nm; in the case of Mo/C, the Mo layer thickness ranged from 1 to 8 nm while the C layer thickness ranged from 0.5 to 2.5 nm; in the case of W/Si, the W layer thickness ranged from 1 to 6.5 nm while the Si layer thickness ranged from 1 to 6 nm. These particular thickness ranges were chosen so that the as-deposited film stresses varied from compressive to tensile, as will be described below. The multilayer films each contain a total of 40 bilayers.

In-plane stress measurements of the as-deposited films were made using the wafer-curvature technique, with an instrument that has been described previously.<sup>20</sup> With this technique, the film stress,  $\sigma$ , is determined from the measured change in radius of curvature,  $R$ , of the thin substrate using Stoney's equation,<sup>21</sup>

$$\sigma = \frac{Y_s t_s^2}{6 t_f R}, \quad (1)$$

where  $t_f$  is the film thickness,  $t_s$  is the substrate thickness, and  $Y_s$  is the biaxial elastic modulus of the substrate (which is related by  $Y_s = E_s / (1 - \nu_s)$  to Young's modulus,  $E_s$ , and Poisson's ratio,  $\nu_s$ , for the substrate). Substrate thicknesses were measured with a micrometer, and film thicknesses were determined from x-ray reflectance analysis.<sup>19</sup> (That is, the multilayer period  $d$  was determined, within a precision of better than  $\pm 0.1$  nm, by fitting the measured x-ray reflectance versus grazing-incidence angle data, and the total film thickness was then computed from  $t_f = 40d$ . The measurements were made using the x-ray diffractometer described below.) A value of  $Y_s = 180$  GPa for Si was used.<sup>22</sup> With the wafer-curvature apparatus, the deflection of a HeNe laser beam is measured as it is scanned along the substrate surface, and the deflection is used to compute the substrate radius; measurements made on the substrate prior to film deposition are used to determine figure errors and thickness variations in the substrate which are then subtracted from subsequent measurements to improve the measurement accuracy. The net precision of the film stress measurements is estimated to be approximately  $\pm 5\%$ .

In the case of the Mo/Si and W/Si films, the stresses in selected samples were also measured as a function of tem-

perature during thermal cycling to 300 °C. The samples were heated in a low-pressure ( $\sim 50$  mTorr) nitrogen atmosphere from room temperature to 300 °C at a rate of 25 °C/min, then held at 300 °C for a period of 5 min, and finally allowed to cool to room temperature over a period of approximately 35 min, assisted by the use of a LN<sub>2</sub> cold finger.

XRD measurements of selected samples were made with a four-circle diffractometer, using a rotating anode Cu source and a pyrolytic graphite monochromator tuned to the Cu  $K\alpha$  line near 8 keV ( $\lambda = 0.154$  nm). Diffraction measurements were made in  $\theta - 2\theta$  geometry over the range of  $33^\circ < 2\theta < 50^\circ$ , sufficient to measure the Mo(110) diffraction peak in the case of Mo/Si and Mo/C films, and the  $\alpha$ -W(110) and  $\beta$ -W(200) peaks in the case of W/Si films.

### III. RESULTS

#### A. Mo/Si multilayers

Shown in Fig. 1(a) is a parametric stress contour plot determined for the as-deposited Mo/Si multilayer films described above: each yellow square corresponds to the stress measured in a particular multilayer film, whose Si layer thicknesses are given by the position of the square along the horizontal axis, and whose Mo layer thicknesses are given by the position along the vertical axis. Smooth "isostress" contours were computed using bilinear interpolation,<sup>23</sup> and are labeled in units of MPa. For example, the stress measured for a Mo/Si multilayer containing 3-nm-thick Si layers and 4-nm-thick Mo layers (having 40 periods) is approximately +300 MPa (tensile). As indicated by the color bar in Fig. 1, compressive stresses are shown in shades of red and tensile stresses in shades of blue.

Although there are certainly errors associated with the bilinear interpolation algorithm used to produce the contours shown in Fig. 1, these contours nonetheless illustrate the general trends. Specifically, the net stress in these particular multilayer structures evidently can be either compressive or tensile, depending on the specific Mo and Si layer thicknesses. This can be understood qualitatively as follows: the net stress,  $\sigma_{ML}$ , in an A/B multilayer stack of period  $d$  is equal to the stresses in the individual A and B layers, weighted by their relative layer thicknesses (neglecting any interfacial stresses):

$$\sigma_{ML}d = \sigma_A d_A + \sigma_B d_B, \quad (2)$$

where  $d_A$  and  $d_B$  are the A and B layer thicknesses, and  $\sigma_A$  and  $\sigma_B$  are the A and B layer stresses, respectively. So if the A layers are compressive, for example, and the B layers tensile (and neglecting, for the moment, the possibility that these stresses might be dependent on the individual A and B layer thicknesses), then the net stress in the film can be either compressive or tensile (or zero), depending on the relative A and B layer thicknesses. Considering that the net stresses measured in the as-deposited films shown in Fig. 1(a) are indeed compressive for smaller Mo layer thicknesses and tensile for larger Mo layer thicknesses, we can infer that the

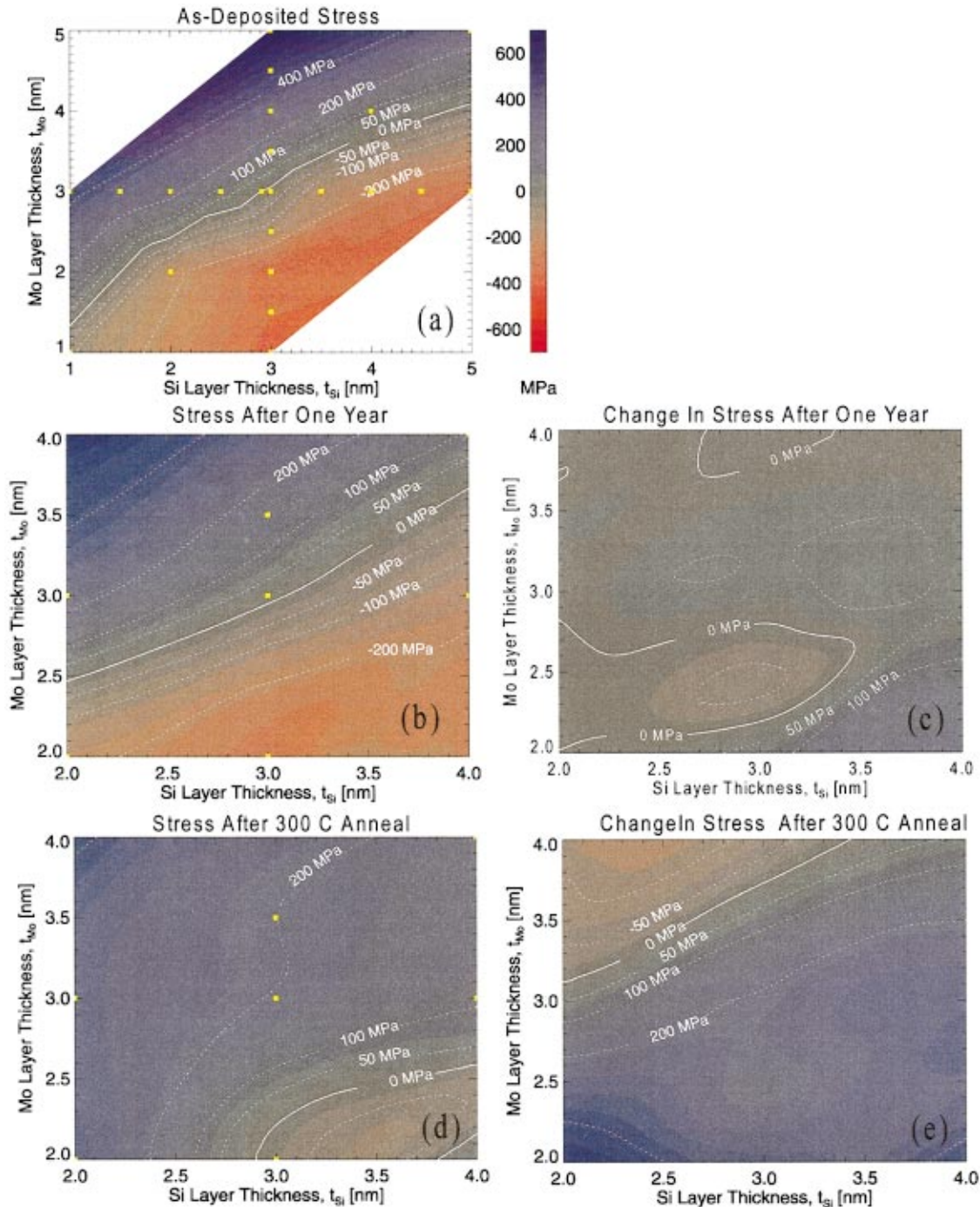


FIG. 1. Parametric stress contour plots for as-deposited Mo/Si multilayer films (a), for the same films after storage in air at room temperature for one year (b), and after thermal cycling to 300 °C (d). The change in stress after storage in air and thermal cycling are shown in (c) and (e), respectively.

Mo layers are in tension and the Si layers in compression, consistent with previous investigations for Mo/Si multilayers.<sup>12,17</sup>

Figure 1(b) is the parametric stress contour plot associated with the same films used in Fig. 1(a), but the stresses in this case were measured after these films were stored in air at room temperature for a period of 12 months; shown in Fig. 1(c) is the net change in stress, i.e., the difference between the stresses shown in Fig. 1(b) and the stresses shown in Fig. 1(a). The stress changes are of order 50 MPa (at most), can

be either compressive or tensile, and there does not appear to be any systematic variation with layer thickness. [Note: The stress contour plots shown in Figs. 1(b)–1(e), as well those shown in Fig. 6, are displayed over a more narrow range of layer thicknesses than was actually used to compute the smooth isostress contours by bilinear interpolation as described in the text. Thus the contours shown Figs. 1(b) and 1(d), for example, were computed from stress measurements made on a total of 13 samples, not just the 7 samples visible (as yellow squares) in the plots.]

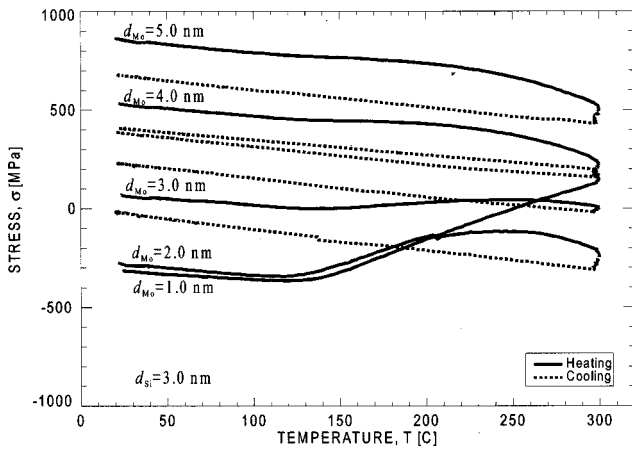


FIG. 2. Stress-temperature curves for Mo/Si multilayer containing 3.0-nm-thick Si layers and for various Mo layer thicknesses.

Figure 1(d) is the parametric stress contour plot for these same films after thermal cycling to 300 °C; the change in stress (relative to the as-deposited stresses) is shown in Fig. 1(e). The stress changes can be as large as ~200 MPa in certain films, and are again either compressive or tensile, but in this case there is a clear dependence on Mo and Si film thickness: multilayers containing thicker Mo layers and thinner Si layers became more compressive, while those with thinner Mo layers and thicker Si layers became more tensile after thermal cycling.

Typical stress-temperature curves are shown in Fig. 2 for Mo/Si multilayers containing 40 bilayers with 3-nm-thick Si layers and Mo layer thicknesses in the range of 1–5 nm. For comparison, stress-temperature curves for 300-nm-thick single-layer Si and Mo films (deposited under conditions identical to those used for multilayer growth described above) are shown in Figs. 3(a) and 3(b), respectively. The linear cooling curves in all cases represent the difference in

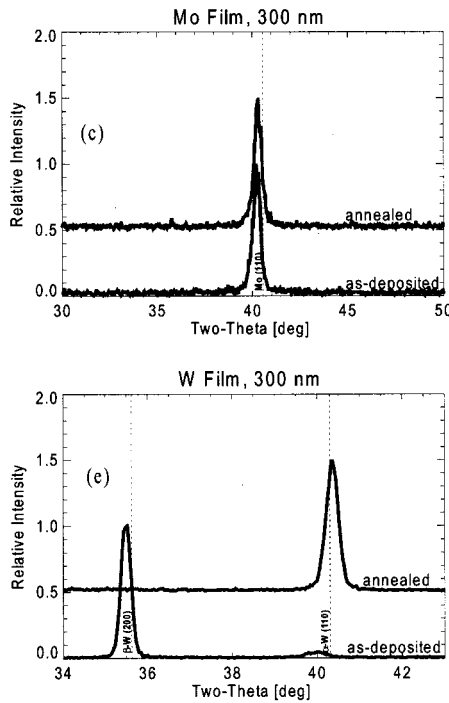
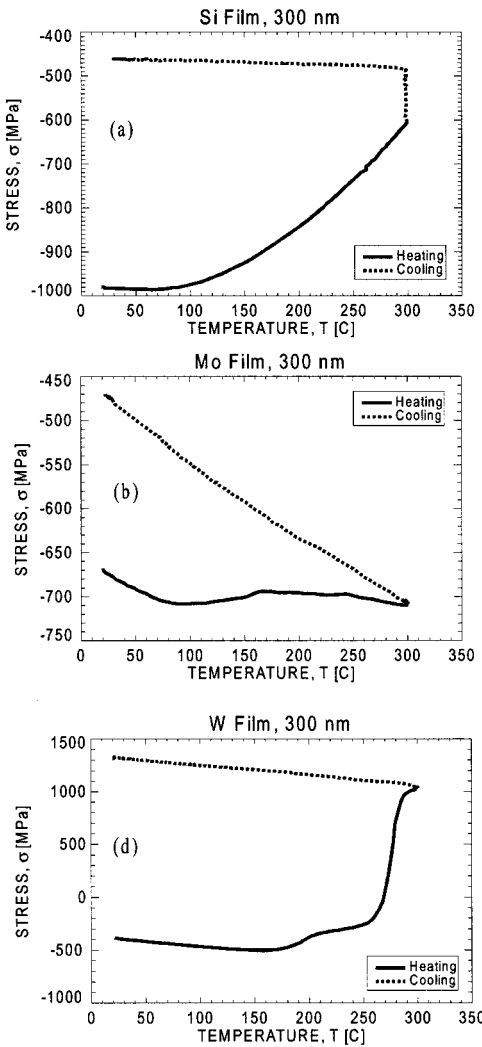


FIG. 3. Stress-temperature curves for 300-nm-thick films of sputtered Si (a), Mo (b), and W (d). XRD data are also shown for as-deposited and annealed films of Mo (c) and W (e).

the coefficient of thermal expansion (CTE),  $\alpha$ , between the film ( $\alpha_{\text{film}}$ ) and the Si substrate ( $\alpha_{\text{Si}}$ ). That is, the slope of the cooling curve is given by

$$\frac{d\sigma}{dT} = -\frac{E_{\text{film}}}{(1-\nu_{\text{film}})}(\alpha_{\text{film}} - \alpha_{\text{Si}}), \quad (3)$$

where  $E_{\text{film}}$  and  $\nu_{\text{film}}$  are the values of Young's modulus and Poisson's ratio of the film. Thus from Figs. 3(a) and 3(b) we find  $\alpha_{\text{Mo}} = 4.9 \pm 0.2 \times 10^{-6}/^{\circ}\text{C}$  and  $\alpha_{\text{Si}} = 3.2 \pm 0.2 \times 10^{-6}/^{\circ}\text{C}$  (using  $E_{\text{Mo}} = 1.6 \times 10^5 \text{ MPa}$ ,  $\nu_{\text{Mo}} = 0.3$ ,  $E_{\text{Si}} = 1.6 \times 10^5 \text{ MPa}$ , and  $\nu_{\text{Si}} = 0.1$ ),<sup>24</sup> which compares favorably with the values of  $\alpha_{\text{Mo}} = 5.2 \times 10^{-6}/^{\circ}\text{C}$  and  $\alpha_{\text{Si}} = 2.9 \times 10^{-6}/^{\circ}\text{C}$  in Ref. 24. The average CTE value for the Mo/Si multilayers determined from Fig. 2 is approximately  $5.8 \pm 0.4 \times 10^{-6}/^{\circ}\text{C}$ , somewhat higher than the average value expected from the rule of mixtures using the CTE values of pure Mo and Si.

Irreversible stress changes occur at a temperature of approximately  $130^{\circ}\text{C}$  during heating in each Mo/Si film shown in Fig. 2. In the case of the single-layer films (Fig. 3), large, irreversible stress changes were also observed during heating, beginning at a temperature of  $\sim 80^{\circ}\text{C}$  for both Mo and Si; the signatures of these changes are evident in the multilayer stress–temperature curves (Fig. 2). In contrast to the results for Mo/Si multilayers, however, where stress changes after annealing can be either tensile or compressive, in both single-layer films the stress changes resulted in more tensile films. The results shown in Figs. 2 and 3 suggest, therefore, that in addition to stress changes occurring in the individual Mo and Si layers, a large part of the irreversible stress changes observed in the multilayer films [Figs. 1(d), 1(e), and 2] is due to some other multilayer-specific mechanism, such as stress changes resulting from diffusion across, or possible growth of the amorphous Mo–Si interlayers present in these structures.<sup>25</sup> Grazing incidence x-ray reflectance measurements made on as-deposited versus annealed samples revealed no observable changes in the multilayer Bragg peaks, as would be expected if there were large structural changes in the interfaces; this result is consistent with previous investigations<sup>26</sup> of the microstructural changes in the amorphous Mo–Si interlayers resulting from thermal cycling, in which no observable changes were observed up to  $300^{\circ}\text{C}$  [as determined by transmission electron microscopy (TEM) and x-ray scattering analyses]. These results suggest, therefore, that diffusion across the interface (below the level of detection by x-ray reflectance analysis) contributes to the observed stress changes more than interface growth does.

The XRD data for selected as-deposited and annealed Mo/Si multilayer films are shown in Fig. 4. The centroid position and the width of the Mo (110) diffraction peaks were determined in each case by fitting these peaks with a Gaussian. Grain sizes were then determined from the Gaussian widths using the Scherrer equation,<sup>27</sup> and are shown in Fig. 5(a) for the as-deposited films containing 3-nm-thick Si layers and in Fig. 5(b) for those containing 3-nm-thick Mo layers; out-of-plane lattice spacings were determined from the centroid positions using Bragg's law, and are shown in Fig. 5(c) for the films containing 3-nm-thick Si layers and in

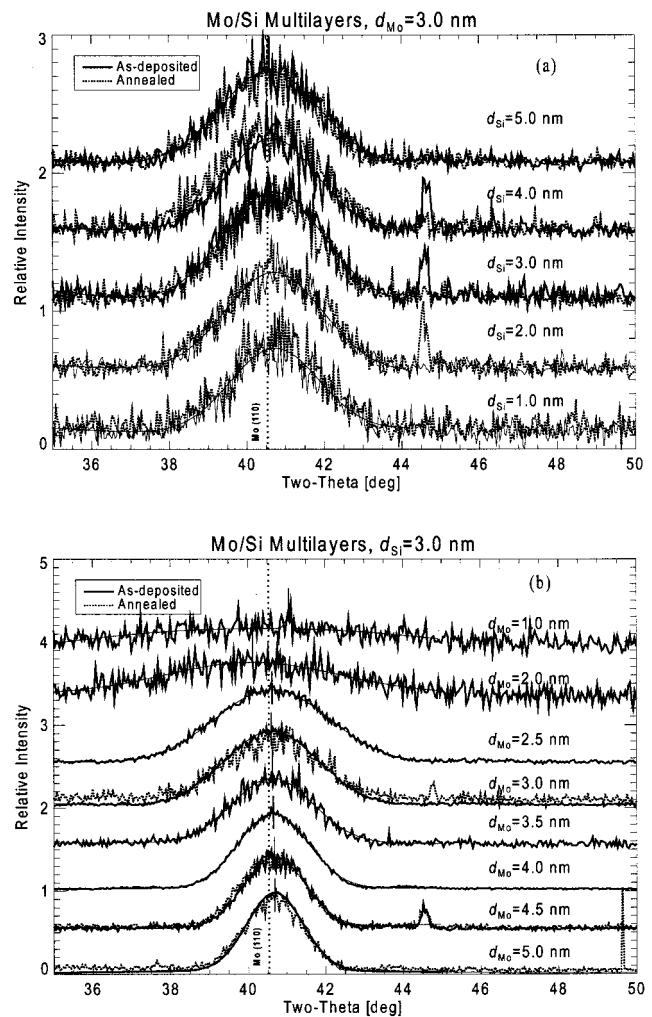


Fig. 4. XRD data for selected as-deposited and annealed Mo/Si multilayers containing 3-nm-thick Mo layers (a) and 3-nm-thick Si layers (b). (The sharp peaks near  $2\theta = 44.5^{\circ}$  present in some scans are due to diffraction from the aluminum sample holder.) The vertical dotted lines indicate the value of  $2\theta$  for which diffraction from bulk Mo (110) is expected. Gaussian fits to the Mo (110) diffraction peaks are shown as smooth lines, and the centroids of these fits are denoted by vertical lines.

Fig. 5(d) for those containing 3-nm-thick Mo layers. From Figs. 5(a) and 5(b), it is clear that the Mo grain size (along the growth direction) is approximately equal to the Mo layer thickness (within experimental uncertainty) in each multilayer film. From Figs. 5(c) and 5(d), we can see that in all cases the out-of-plane lattice spacings are smaller than the bulk value for Mo, suggesting that the in-plane stresses in the Mo layers are tensile, consistent with the wafer-curvature results. We also observe with some surprise that the Mo (110) lattice spacing tends towards the bulk value for thinner (rather than thicker) Mo layers, as well as for thicker Si layers. The observed variations in lattice spacing with layer thickness can be due to a number of effects, i.e., the substrate-interaction and interface-contraction effects discussed in Sec. IV; in particular, (thickness-dependent) Si diffusion into the Mo layers could easily alter the lattice spacing of the Mo crystallites enough to explain the XRD results

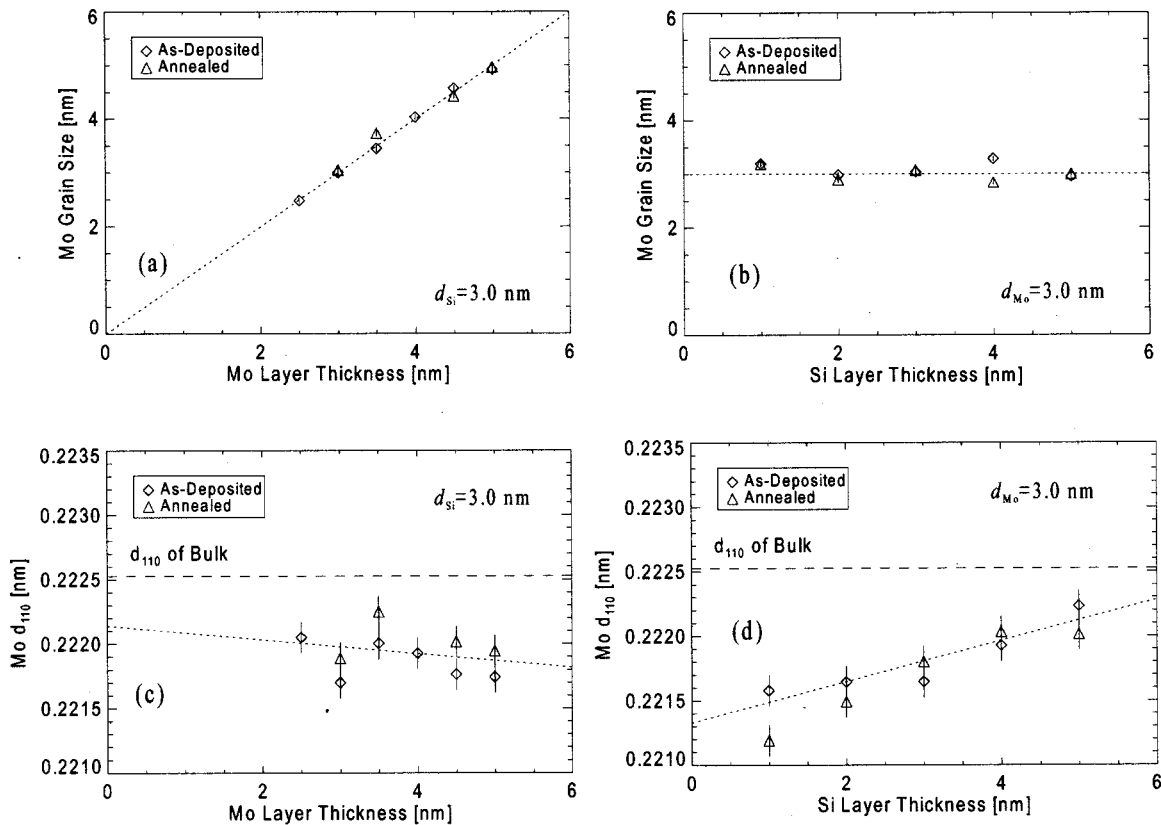


FIG. 5. Mo grain sizes [(a) and (b)], and Mo (110) lattice spacings [(c) and (d)], determined from the x-ray data in Fig. 4, for as-deposited Mo/Si films containing 3.0-nm-thick Si layers as a function of Mo layer thickness, and for films containing 3.0-nm-thick Mo layers as a function of the Si layer thickness indicated. Dotted lines are guides to the eye.

shown in Fig. 5. In any case, these results demonstrate conclusively that the strains in the Mo layers are dependent on the thicknesses of both the Mo and the Si layers, thus complicating significantly the simple model described above [i.e., Eq. (2)] for the net stress in a multilayer, which neglects any possible variation in stress with thickness for the individual layers that comprise the multilayer stack. Furthermore, the observation that the as-deposited stress in the Mo single-layer film is compressive while the stresses in the Mo layers comprising the Mo/Si multilayers are tensile indicates that the stresses in these Mo layers are highly dependent on their local environment.

The XRD data (Fig. 5) were not used for quantitative analysis of the stresses in the individual Mo layers in the Mo/Si multilayers, as such an approach is unwarranted in this case. The out-of-plane strain,  $\epsilon$ , is related to the (out-of-plane) lattice spacing,  $d$ , and the “relaxed” lattice spacing,  $d_0$  (which is not necessarily equal to the bulk lattice spacing) according to

$$\epsilon = \frac{d - d_0}{d_0}, \quad (4)$$

while the in-plane stress,  $\sigma$ , is related to the out-of-plane strain by

$$\sigma = -\frac{E}{2\nu} \epsilon = -\frac{E}{2\nu} \frac{(d - d_0)}{d}. \quad (5)$$

Thus, in principle, we could compute the stresses in the individual Mo layers that comprise the Mo/Si multilayers from the lattice spacings determined from XRD, and we could then compute the stresses in the Si layers by subtracting the Mo layer stresses so derived from the net multilayer stresses measured by wafer curvature. However the large uncertainty in our knowledge of the relaxed lattice spacing  $d_0$  (as well as the large uncertainties in the measured Mo lattice spacings) results in uncertainties in the Mo layer stresses that are far too large for meaningful conclusions to be drawn. Thus, unlike the case of polycrystalline metallic multilayers, where it was possible to determine the complete stress state of the individual layers using detailed x-ray diffraction measurements,<sup>28</sup> such an approach is not practical in the case of the multilayer structures considered here containing amorphous Si or C layers.

## B. W/Si multilayers

Shown in Fig. 6 are the parametric stress contour plots for W/Si multilayer films. Similar to the Mo/Si data shown in Fig. 1, Fig. 6(a) shows the as-deposited stresses, while Figs. 6(b) and 6(c) show the stresses and stress changes observed in these films after storage in air at room temperature, in this case for a period of four months; the stresses and stress changes observed upon thermal cycling to 300 °C are shown in Figs. 6(d) and 6(e). Like the dependence with Mo layer

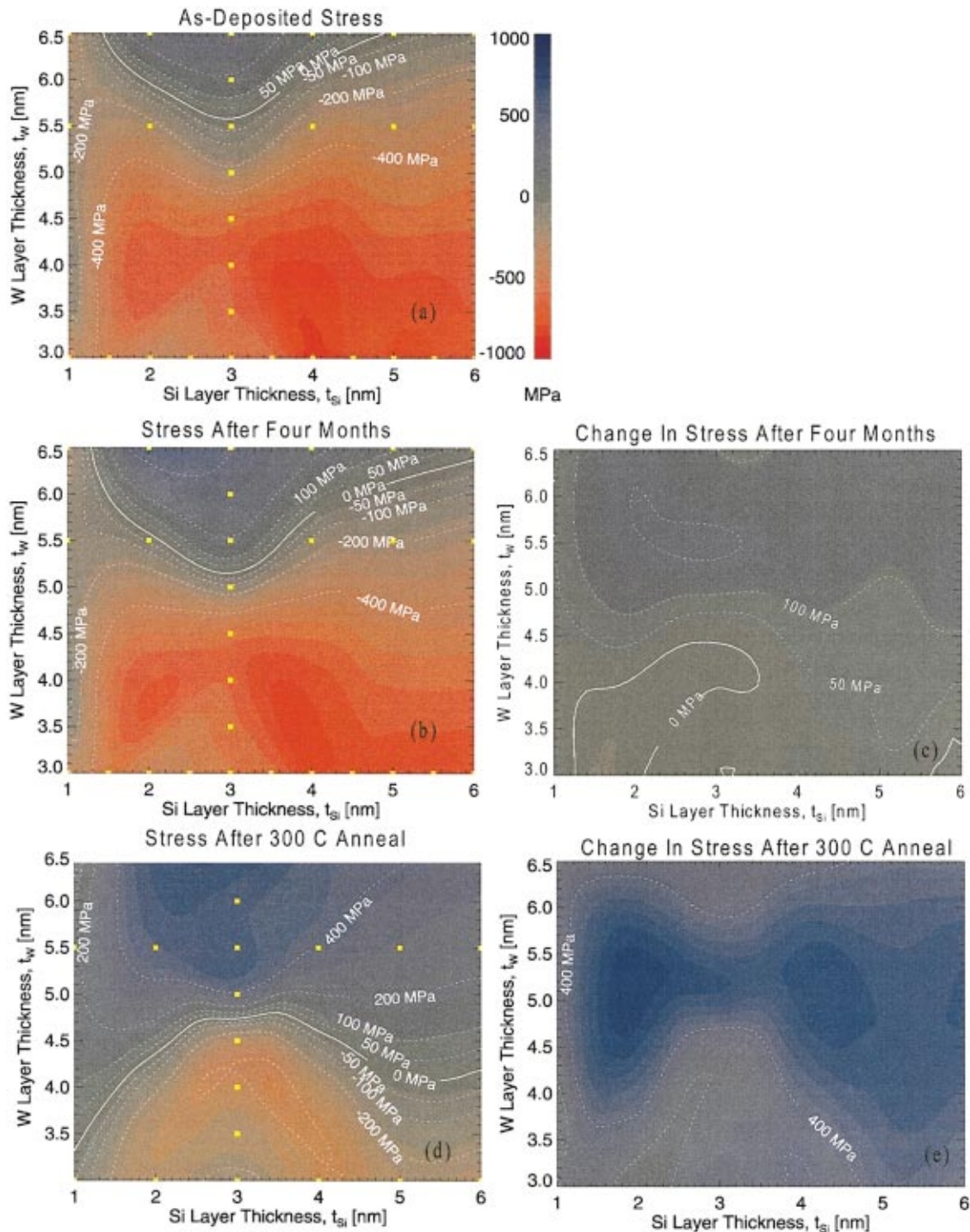


FIG. 6. Parametric stress contour plots for as-deposited W/Si multilayer films (a), for the same films after storage in air at room temperature for one year (b), and after thermal cycling to 300 °C (d). The change in stress after storage in air and thermal cycling are shown in (c) and (e), respectively.

thickness observed in Mo/Si, compressive stresses are observed in the as-deposited films for thinner W layer thicknesses; unlike Mo/Si, however, the stresses remain compressive for thicker W layers when the Si layer thicknesses are small, i.e.,  $d_{\text{Si}}=1$  nm. Furthermore, the largest stresses are significantly greater than the largest stresses observed in Mo/Si, and the stress changes after storage in air are also larger than in the case of Mo/Si, of order  $\sim 100$  MPa or more for

multilayers containing thicker W layers; the stress changes after annealing are all tensile, with changes in excess of 400 MPa in some cases, also in contrast to Mo/Si (for which the largest stress changes after thermal annealing are of the order of 200 MPa).

Typical stress–temperature curves for selected W/Si multilayer films are shown in Fig. 7; XRD data are shown in Fig. 8, and the lattice spacings derived (for the air-stored

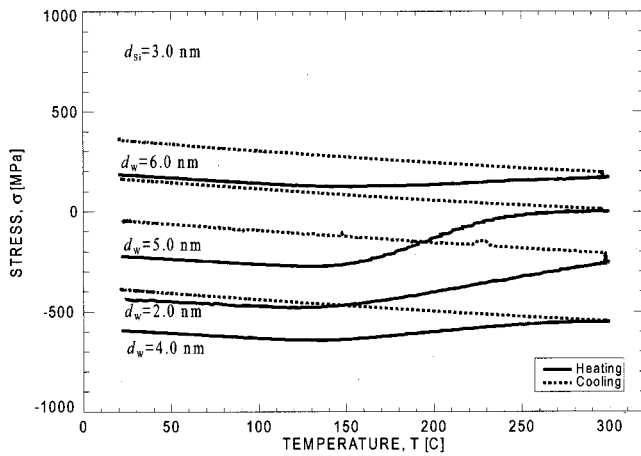


Fig. 7. Stress–temperature curves for W/Si multilayers containing 3.0-nm-thick Si layers and for various W layer thicknesses.

samples) are in Fig. 9. For comparison, the stress–temperature curve obtained for a 300-nm-thick W layer is shown in Fig. 3(d) and the associated x-ray data in Fig. 3(e). In the case of the single-layer W film, irreversible stress changes begin to occur at a temperature of  $\sim 170^\circ\text{C}$ , while irreversible stress changes occur in the W/Si multilayers at temperatures below  $150^\circ\text{C}$ . As indicated in Fig. 3(d), the stress in the single-layer W film changes from compressive to highly tensile after thermal cycling. Similar stress changes in the individual W layers occurring in the W/Si multilayers are no doubt responsible, at least in part, for the observed tensile stress changes, although it is not possible just from the data presented here to separate out any contributions due to interface diffusion or growth of the amorphous W–Si interlayers present in these structures.<sup>29</sup> The average CTE value for the W/Si films determined from the slopes of the cooling curves in Fig. 7 is approximately  $4.5 \pm 0.3 \times 10^{-6}/^\circ\text{C}$ , again somewhat higher than the average value expected from the rule of mixtures using the CTE values of pure Si and W. [The CTE value for W determined from Fig. 3(d) was found to be  $\alpha_W = 4.5 \pm 0.2 \times 10^{-6}/^\circ\text{C}$ , consistent with the value of  $\alpha_W = 4.8 \times 10^{-6}/^\circ\text{C}$  given in Ref. 24].

The XRD data presented in Fig. 3(e) show that the as-deposited W film consists predominantly of the  $\beta$  phase of W, as indicated by the  $\beta$ -W (200) Bragg peak near  $2\theta = 35^\circ$ , although a small amount of the  $\alpha$  phase is present, as indicated by the broad, weak  $\alpha$ -W (110) peak near  $2\theta = 40.5^\circ$ . In contrast, the annealed film is characterized by a sharp  $\alpha$ -W (110) peak, and there is no evidence of any  $\beta$ -phase material at all. We note that the positions of the  $\alpha$ - and  $\beta$ -phase Bragg peaks relative to the positions of the peaks expected for bulk material are qualitatively consistent with a compressive stress state in the as-deposited film, and with a tensile stress state in the annealed film, but we refrain from making any quantitative statements for the same reasons presented above in the discussion of Mo strains and stresses.

Turning now to the x-ray data for the W/Si multilayer

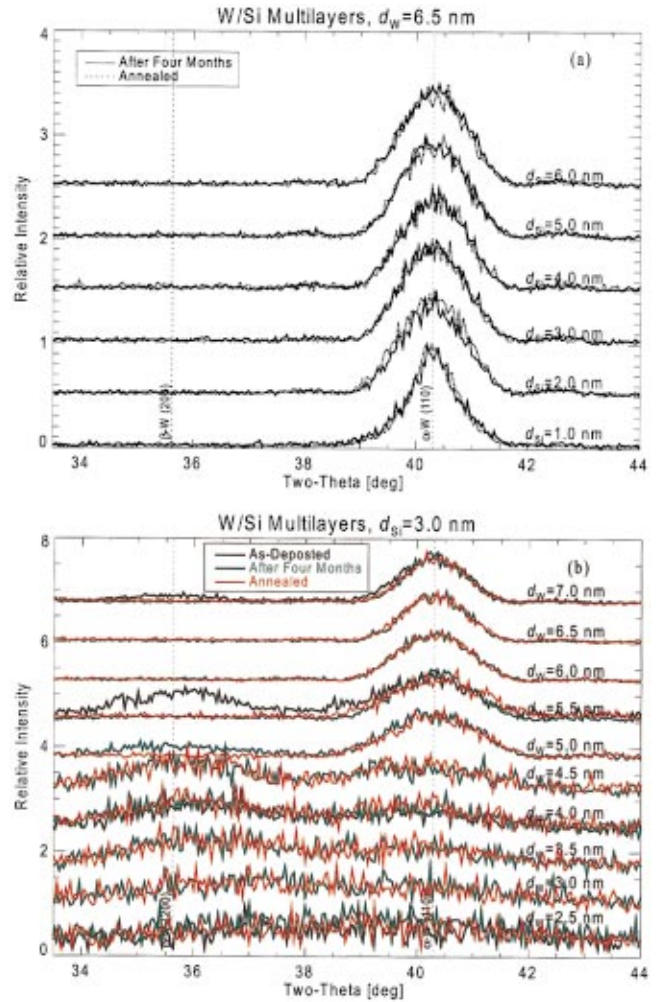


Fig. 8. XRD data for selected as-deposited, stored in air, and annealed W/Si multilayers containing 3-nm-thick W layers (a) and 3-nm-thick Si layers (b). The vertical dotted lines indicate the values of  $2\theta$  for which diffraction from bulk  $\alpha$ -W (110) and  $\beta$ -W (200) is expected. Gaussian fits to the diffraction peaks are shown as smooth lines, and the centroids of these fits are denoted by vertical lines.

films presented in Figs. 8 and 9, we note that the relative intensities of the  $\alpha$ - and  $\beta$ -phase peaks in the as-deposited films containing 3-nm-thick Si layers vary strongly as a function of W layer thickness: the  $\beta$  phase is evident in all the as-deposited films, and in contrast to the single-layer W film, is also present in the air-stored and annealed films having W layer thicknesses of 4.5 nm or less. The W/Si multilayer containing 5-nm-thick W layers is evidently a marginal case: the  $\beta$  phase survives air storage, but not  $300^\circ\text{C}$  thermal cycling. The out-of-plane lattice spacings for both the  $\alpha$ - and  $\beta$ -phase material in these films, shown in Fig. 9, suggest that the  $\alpha$  phase becomes more compressive, while the  $\beta$  phase more tensile, as the W layer thickness decreases; we note, however, that because these films are so thin, the signal-to-noise ratio is quite low in the XRD data (Fig. 9) for the W/Si films containing the thinnest W layers (i.e., for  $d_W < 4$  nm). Consequently the uncertainties in the derived lattice spacings are large, and so this conclusion must be considered as tentative. Nonetheless, as in the case of the Mo layers in the

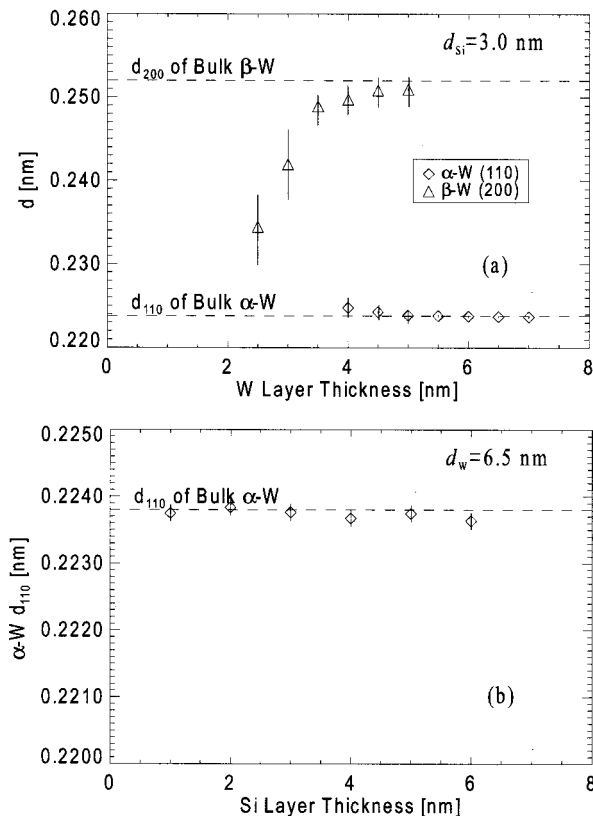


FIG. 9. W lattice spacings determined from the x-ray data in Fig. 8, for air-stored W/Si films containing 3.0-nm-thick Si layers as a function of W layer thickness (a), and for films containing 3.0-nm-thick W layers as a function of Si layer thickness (b).

Mo/Si multilayers described above, we note that the strains in the W layers clearly depend on W layer thickness; this result also could be explained by thickness-dependent diffusion.

### C. Mo/C multilayers

The parametric stress contour plot for as-deposited Mo/C multilayers is shown in Fig. 10. These data are similar to those for Mo/Si shown in Fig. 1(a): compressive stresses are observed for films containing thicker C layers and thinner Mo layers, and tensile stresses for thinner C layers and thicker Mo layers, suggesting tensile Mo layers and compressive C layers. The XRD data for selected Mo/C films are shown in Fig. 11, and the Mo lattice spacings derived from these data are shown in Fig. 12. In the case of Mo/C films containing C layers thicker than 0.5 nm, the Mo (110) lattice spacing is larger than the bulk value, suggesting that these Mo layers are in compression, unlike the Mo/Si case, and in apparent conflict with the wafer-curvature results shown in Fig. 10. Again we note, however, that conclusions based on the bulk value for the relaxed lattice parameter are tenuous at best; as in the Mo/Si and W/Si multilayers just discussed, diffusion of C into Mo could substantially alter the lattice spacing of the Mo crystallites and thus explain the XRD results.

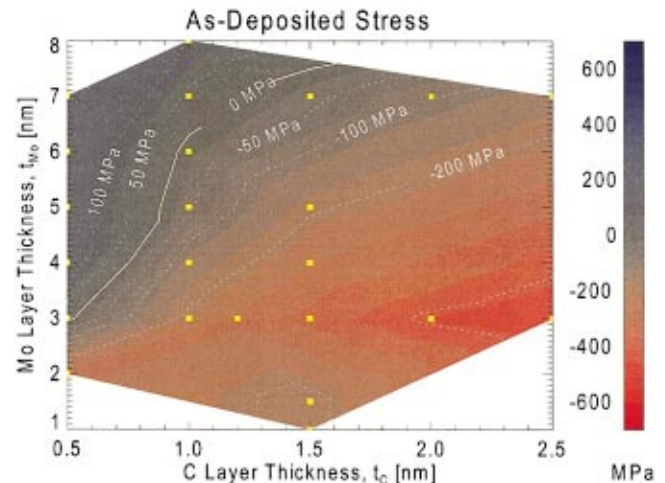


FIG. 10. Parametric stress contour plots for as-deposited Mo/C multilayer films.

In the case of Mo/C films containing 0.5-nm-thick C layers, the XRD data reveal that the Mo layers are at least partially coherent from layer to layer, as indicated by the superlattice peaks apparent in Fig. 11. The coherency of the Mo layers is evidently correlated with the tensile stress state observed in all but one of the as-deposited films containing 0.5-nm-thick C layers.

## IV. DISCUSSION

As discussed in detail by Bain *et al.*,<sup>28</sup> stresses in multilayers can be classified as substrate-interaction stresses, coherency stresses, and interfacial-contraction stresses. A number of possible mechanisms that give rise to stresses from each of these three classes can be invoked to explain the net film stresses reported above in as-deposited, aged, and thermally cycled Mo/Si, W/Si, and Mo/C multilayers (Figs. 1, 6, and 10, respectively), which clearly cannot be described adequately by Eq. (2) as it is written, i.e., assuming thickness-independent layer stresses, and neglecting both interlayer and interfacial stresses. We now discuss some of these mechanisms.

Substrate-interaction stresses usually result from volume changes (associated with alloying, defect annihilation, grain growth, island agglomeration, differential thermal expansion, etc.) that are opposed by the substrate. Such stresses can vary with layer thickness as a result of stress evolution during growth, in which case the net multilayer stress [i.e., Eq. (2)] cannot be described using thickness-independent A and B layer stresses; rather, we must take  $\sigma_A = \sigma_A(d_A, d_B)$  and/or  $\sigma_B = \sigma_B(d_A, d_B)$  (here A/B=Mo/Si, W/Si, or Mo/C). Thickness-dependent substrate-interaction stresses can also arise during growth from the action of surface stresses (resulting from the free-energy decrease associated with a reduction in surface area), an effect which plays an increasingly smaller role as the film thickens.

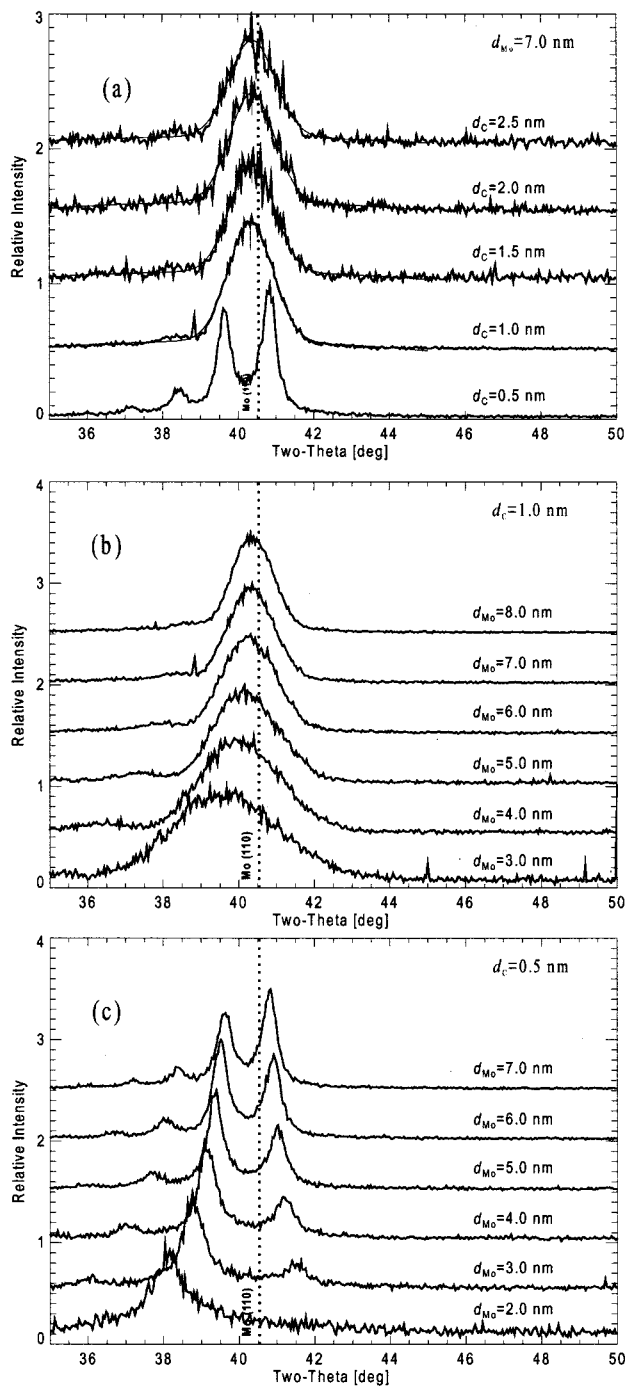


FIG. 11. XRD data for selected Mo/C multilayers, containing 7-nm-thick Mo layers (a) 1.0-nm-thick C layers (b), and 0.5-nm-thick C layers. The vertical dotted lines indicate the value of  $2\theta$  for which diffraction from bulk Mo (110) is expected.

The most important thickness-dependent stress-evolution mechanisms for the sputtered films considered here are likely to be volume changes resulting from energetic bombardment and/or diffusion. Films deposited by low-pressure magnetron sputtering are subject to a large energy input during growth through collisions with energetic incident adatoms, Ar atoms, and Ar ions.<sup>30</sup> Consequently, large compressive stresses can be produced through the so-called “atomic peening”

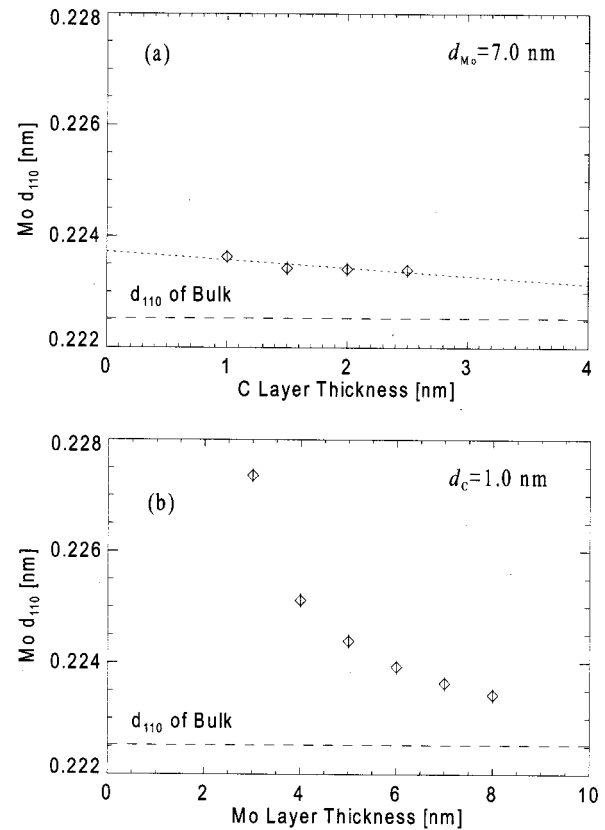


FIG. 12. Mo (110) lattice spacings determined from the x-ray data in Fig. 11, for as-deposited Mo/C films containing 7.0-nm-thick Mo layers as a function of C layer thickness (a), and for films containing 1.0-nm-thick C layers as a function of Mo layer thickness (b).

effect.<sup>31</sup> Thus the stress in a layer can evolve with thickness due to atomic peening (which can cause churning of atoms within 1.0–1.5 nm of the surface<sup>29</sup>) because thicker layers are subjected to longer periods of bombardment by energetic atoms and ions. Furthermore, the stress in an A layer can change during deposition of the subsequent B layer, since the underlying A layer will be subjected to bombardment (with the possibility of resputtering as well as churning<sup>29</sup>) by energetic B adatoms, Ar ions, and especially neutral Ar atoms reflected from the B target; the resultant stress in the A layer can thus depend on the B layer thickness because thicker B layers will result in longer bombardment times. Volume changes resulting from diffusion during growth can also result in thickness-dependent layer stresses. For instance, the amount of diffusion of A atoms into adjacent B layers will be greater, in general, for thicker B layers, and *visa versa*.

But whatever the mechanism, thickness-dependent stress variations in thin films are typically associated with morphology variations as well. For example, Vink *et al.* have measured the evolution with thickness of stress and microstructure in sputtered Mo (Ref. 32) and W (Ref. 33) films using XRD and electron microscopy. [However, we note that in the case of W, Vink *et al.* found predominantly  $\alpha$ -phase material in compressive films, and  $\beta$ -phase material in tensile films, in contrast to the present results for W films in Fig.

3 and the W/Si multilayers in Fig. 8(b).] The XRD results presented above for the case of multilayer films also indicate clear changes in microstructure with layer thickness for the Mo and W layers in Mo/Si, W/Si, and Mo/C structures. These results suggest, therefore, that the observed thickness-dependent multilayer stresses are due, at least in part, to thickness-dependent stresses in the individual metal layers.

In addition to thickness-dependent stresses resulting from energetic bombardment and diffusion, the formation and subsequent growth over time or at elevated temperatures of A–B interlayers of mixed composition can contribute to the net substrate-interaction stress in A/B multilayers as well. These interlayers, i.e., the amorphous Mo–Si layers found in Mo/Si multilayers<sup>25</sup> and W–Si layers found in W/Si multilayers,<sup>29</sup> contribute an amount  $\sigma_{AB}d_{AB}$  to the net film stress, where  $\sigma_{AB}$  is the stress in the A–B interlayer, and  $d_{AB}$  is the interlayer thickness. The interlayer stress contribution can be substantial: Kassner *et al.*<sup>16</sup> reported a residual stress of  $-1.8$  GPa (compressive) in the  $\sim 1$ -nm-thick Mo–Si interlayers present in as-deposited [Mo(3 nm)/*a*-Si(4 nm)]  $\times 40$  multilayers, as compared to the 1.2–2.0 GPa (tensile) stresses they found in the Mo layers and the  $-1.3$  GPa (compressive) stresses in the *a*-Si layers. Furthermore, subsequent growth (with time and/or temperature) of the A–B interlayers can result in changes in the net film stress through volume changes in the A and/or B layers as well as in the interlayers themselves. As discussed already in Sec. III, such changes in the Mo–Si and W–Si interlayers, along with diffusion across the interfaces, can explain in part the observed changes in stress with time and temperature in the Mo/Si (Figs. 1 and 2) and W/Si (Figs. 6 and 7) multilayers.

Multilayer coherency stress, resulting from lattice mismatch strains between adjacent layers, only applies to the coherent Mo/C multilayers described above (i.e., those having  $d_C = 0.5$  nm and  $d_{Mo} > 2$  nm) and presumably is responsible (at least in part) for the tensile stresses observed in these films; multilayer coherency stress does not apply to the remaining polycrystalline/amorphous Mo/Si, W/Si, and Mo/C multilayers considered here.

Interfacial-contraction (or -dilation) stresses, due to interface forces analogous to surface tension, have been postulated to play a role in multilayers;<sup>34</sup> the contribution of such stresses to the net film stress will diminish with decreasing interface density (i.e., with increasing bilayer thickness), and might therefore explain some of the observed thickness-dependent stresses reported here. However, although interfacial stresses have been measured in textured metallic Ag/Ni multilayers having sharp interfaces,<sup>35</sup> it remains unclear if such stresses are significant in the case of multilayers known to have diffuse interfaces, such as the Mo/Si and W/Si structures considered here.

Although specific combinations of some of the mechanisms just described undoubtedly can be used to explain the net film stresses reported here in as-deposited, aged, and thermally annealed multilayers, without a more complete determination of the stress state in the individual layers that comprise the multilayer structures it is not possible to ascer-

tain, quantitatively, the relative contributions of each possible effect. Such an analysis, as was done, for example, by Bain *et al.* using wafer-curvature measurements combined with grazing incidence and asymmetric x-ray diffraction measurements for the case of metallic Mo/Ni multilayers,<sup>28</sup> is difficult if not impossible in the case of polycrystalline/amorphous multilayer structures. Perhaps the future development of more sensitive techniques to determine the stress state in the individual polycrystalline and amorphous layers that comprise the multilayers considered here could be used to solve this problem conclusively.

## V. CONCLUSIONS

The results for Mo/Si, W/Si, and Mo/C multilayer films presented here indicate that the stresses in these structures are neither intrinsic nor stable, in general. Rather, the net film stress (a) depends on the thicknesses of the individual layers that comprise the multilayer, and (b) can change over time, even at room temperature. A number of possible mechanisms have been discussed in order to explain these results, including thickness-dependent stresses resulting from diffusion and energetic bombardment during growth, coherency stresses, interfacial stresses, and stresses associated with the formation and subsequent growth of amorphous interlayers.

The present results—taken along with previous investigations of the stresses in Mo/Si multilayers which revealed that the net film stress also depends strongly on deposition conditions such as argon pressure<sup>13</sup> and even on the background pressure in the vacuum system prior to deposition<sup>13</sup>—suggest that there are indeed many parameters that can be adjusted, in principle, in order to achieve a low-stress film, as is required for high-performance multilayer x-ray optics. But, on the other hand, these same results also indicate that finding the precise set of deposition parameters that give rise to a low-stress film will be a difficult task, in general, and even then, the observed stress changes with time and temperature reported here show that it will be difficult to maintain a specific stress state over time under the conditions typically associated with the application of multilayer x-ray optics (e.g., space-borne telescopes, high-power synchrotron beamlines, high-throughput lithography systems, etc.). It seems necessary, therefore, to develop low-temperature thermal cycling procedures suitable for use on coated, precision substrates, as well as other possible stress-reduction techniques, such as those described by Tinone *et al.*<sup>36</sup> and by Mirkarimi,<sup>37</sup> that can be used to stabilize the stresses present in these films.

## ACKNOWLEDGMENTS

The author would like to acknowledge useful discussions with R. C. Cammarata of Johns Hopkins University and with W. L. Brown of Bell Labs, who also provided a careful review of this manuscript.

<sup>1</sup>F. A. Doljack and R. W. Hoffman, *Thin Solid Films* **12**, 71 (1972).

<sup>2</sup>J. A. Thornton, *J. Vac. Sci. Technol.* **11**, 666 (1974).

- <sup>3</sup>D. W. Hoffman and J. A. Thornton, *Thin Solid Films* **40**, 355 (1977).
- <sup>4</sup>J. A. Thornton and D. W. Hoffman, *J. Vac. Sci. Technol.* **14**, 164 (1977).
- <sup>5</sup>J. A. Thornton, J. Tabock, and D. W. Hoffman, *Thin Solid Films* **64**, 111 (1979).
- <sup>6</sup>C. T. Wu, *Thin Solid Films* **64**, 103 (1979).
- <sup>7</sup>P. V. Plunkett, R. M. Johnson, and C. D. Wiseman, *Thin Solid Films* **64**, 121 (1979).
- <sup>8</sup>D. W. Hoffman and J. A. Thornton, *J. Vac. Sci. Technol.* **17**, 380 (1980).
- <sup>9</sup>D. W. Hoffman, *Thin Solid Films* **107**, 353 (1983).
- <sup>10</sup>J. A. Thornton and D. W. Hoffman, *J. Vac. Sci. Technol. A* **3**, 576 (1985).
- <sup>11</sup>T. D. Nguyen, *Mater. Res. Soc. Symp. Proc.* **343**, 579 (1994).
- <sup>12</sup>C. A. Volkert, D. L. Windt, W. K. Waskiewicz, J. A. Liddle, and H. A. Huggins, in *The Physics of X-Ray Multilayer Structures*, 1994 Technical Digest Series Vol. 6 (Optical Society of America, Washington, DC, 1994) p. 101.
- <sup>13</sup>D. L. Windt, W. L. Brown, C. A. Volkert, and W. K. Waskiewicz, *J. Appl. Phys.* **78**, 2423 (1995).
- <sup>14</sup>R. R. Kola, D. L. Windt, W. K. Waskiewicz, B. E. Weir, R. Hull, G. K. Celler, and C. A. Volkert, *Appl. Phys. Lett.* **60**, 3120 (1992).
- <sup>15</sup>O. B. Loopstra, E. R. van Sneek, Th. H. de Keijser, and E. J. Mittemeijer, *Phys. Rev. B* **44**, 13519 (1991).
- <sup>16</sup>M. E. Kassner, F. J. Weber, J. Koike, and R. S. Rosen, *J. Mater. Sci.* **31**, 2291 (1996).
- <sup>17</sup>J. M. Freitag and B. M. Clemens, *Appl. Phys. Lett.* **73**, 43 (1998).
- <sup>18</sup>D. L. Windt and W. K. Waskiewicz, *J. Vac. Sci. Technol. B* **12**, 3826 (1994).
- <sup>19</sup>D. L. Windt, *Comput. Phys.* **12**, 360 (1998).
- <sup>20</sup>C. A. Volkert, *J. Appl. Phys.* **70**, 3251 (1991).
- <sup>21</sup>G. G. Stoney, *Proc. R. Soc. London, Ser. A* **82**, 172 (1909).
- <sup>22</sup>W. A. Brantley, *J. Appl. Phys.* **44**, 534 (1973).
- <sup>23</sup>Bilinear interpolation of the stress data was computed using the TRIGRID/QUINTIC procedure included as part of the IDL data language package (Research Systems, Inc., Boulder, CO); in this case Akima's quintic polynomial are used to perform smooth interpolation, as described in *ACM Trans. Math. Softw.* **4**, 148 (1992).
- <sup>24</sup>TAPP ver. 2.0, E S Microwave, Inc., Hamilton, OH.
- <sup>25</sup>R. S. Rosen, D. G. Stearns, M. A. Viliardos, M. E. Kassner, S. P. Vernon, and Y. Cheng, *Appl. Opt.* **32**, 6975 (1993).
- <sup>26</sup>D. G. Stearns, M. B. Stearns, Y. Cheng, J. H. Stith, and N. M. Ceglio, *J. Appl. Phys.* **67**, 2415 (1990).
- <sup>27</sup>B. D. Cullity, *Elements of X-Ray Diffraction* (Addison-Wesley, Reading, MA, 1978).
- <sup>28</sup>J. A. Bain, L. J. Chyung, S. Brennan, and B. M. Clemens, *Phys. Rev. B* **44**, 1184 (1991).
- <sup>29</sup>M. M. Hasan, R. J. Highmore, and R. E. Somekh, *Vacuum* **43**, 55 (1992).
- <sup>30</sup>H. Windischmann, *J. Vac. Sci. Technol. A* **9**, 2431 (1991).
- <sup>31</sup>F. M. D'Heurle, *Metall. Trans.* **1**, 725 (1970).
- <sup>32</sup>T. J. Vink, M. A. J. Somers, J. L. C. Daams, and A. G. Dirks, *J. Appl. Phys.* **70**, 4301 (1991).
- <sup>33</sup>T. J. Vink, W. Walrave, J. L. C. Daams, A. G. Dirks, M. A. J. Somers, and K. J. A. van den Aker, *J. Appl. Phys.* **74**, 988 (1993).
- <sup>34</sup>F. H. Streitz, R. C. Cammarata, and K. Sieradzki, *Phys. Rev. B* **49**, 10707 (1993).
- <sup>35</sup>J. A. Ruud, A. Witvrouw, and F. Spaepen, *J. Appl. Phys.* **74**, 2517 (1993).
- <sup>36</sup>M. C. K. Tinone, T. Haga, and H. Kinoshita, *J. Electron Spectrosc. Relat. Phenom.* **80**, 461 (1996).
- <sup>37</sup>P. B. Mirkarimi, *Opt. Eng. (Bellingham)* **38**, 1246 (1999).